# Effect of Vanadium Addition on the Microstructure, Hardness, and Wear Resistance of $Al_{0.5}CoCrCuFeNi$ High-Entropy Alloy

MIN-RUI CHEN, SU-JIEN LIN, JIEN-WEI YEH, SWE-KAI CHEN, YUAN-SHENG HUANG, and MING-HAO CHUANG

The authors studied the effect of vanadium addition on the microstructure and properties of $Al_{0.5}CoCrCuFeNi$ high-entropy alloy. The microstructure of $Al_{0.5}CoCrCuFeNiV_x$ ($x = 0$ to 2.0 in molar ratio) alloys was investigated by scanning electron microscopy, energy dispersive spectrometry, and X-ray diffraction. With little vanadium addition, the alloys are composed of a simple fcc solid-solution structure. As the vanadium content reaches 0.4, a BCC structure appears with spinodal decomposition and envelops the FCC dendrites. From $x = 0.4$ to 1.0, the volume fraction of bcc structure phase increases with the vanadium content increase. When $x = 1.0$, fcc dendrites become completely replaced by bcc dendrites. Needle-like $\sigma$-phase forms in bcc spinodal structure and increases from $x = 0.6$ to 1.0 but disappears from $x = 1.2$ to 2.0. The hardness and wear resistance of the alloys were measured and explained with the evolution of the microstructure. The hardness values of the alloys increase when the vanadium content increases from 0.4 to 1.0 and peak (640 HV) at a vanadium content of 1.0. The wear resistance increases by around 20 pct as the content of vanadium increases from $x = 0.6$ to 1.2 and levels off beyond $x = 1.2$. The optimal vanadium addition is between $x = 1.0$ and 1.2. Compared with the previous investigation of $Al_{0.5}CoCrCuFeNi$ alloy, the vanadium addition to the alloy promotes the alloy properties.

## I. INTRODUCTION

FOR thousands of years, the development of practical alloy systems has been based mainly on one principal element as the matrix, such as iron-, copper-, and aluminum-based alloys, limiting the number of applicable alloy systems even though a substantial amount of other elements is incorporated of property/processing enhancement.[1,2] The main reason for not incorporating multiprincipal elements into alloy preparation is the anticipated formation of many intermetallic compounds and complex microstructures.[3] Brittleness of the alloys and also difficulty in processing and analysis are expected with the compound formation and complex microstructures, discouraging other new alloy designs with multiprincipal elements.[4]

In recent years, one kind of new alloy, high-entropy alloys with multiple principal elements in equimolar or near-equimolar ratios, has been developed by Yeh *et al.*[4,5] High-entropy alloys may contain principal elements, with the concentration of each element being between 35 and 5 at. pct. Solid solutions with multiprincipal elements tend to be more stable at elevated temperatures because of their large mixing entropies.[4] Following Boltsmann's hypothesis of the relationship between the entropy and system complexity, the change in configurational entropy during the formation of a solid solution from three elements with an equimolar ratio is already larger than the entropy changes for fusion of most metals. Consequently, alloys containing a higher number of principal elements will more easily yield the formation of random solid solutions during solidification, rather than intermetallic compounds or other complicated phases.[4,5,6] $AlCoCrCu_{0.5}Ni$, $Al_xCoCrCuFeNi$, AlCoCrCuFeMoNiTiVZr, $AlCoCrFeMo_{0.5}NiSiTi$, and $AlCrFeMo_{0.5}NiSiTi$ high-entropy alloys are examples exhibiting a quite simple as-cast microstructure and promising properties.[4,7–10]

Among the previous alloys investigated, the $Al_{0.5}CoCrCuFeNi$ alloy is an eminent alloy for structural applications; it has a simple fcc structure and good hot and cold workability. Moreover, it exhibits a wear resistance similar to the 17 to 4 PH stainless steel with hardness around 400 HV due to its large work-hardening capacity, although its as-cast hardness is around 200 HV.[4,8,9,10] However, in accordance with the broadness of high-entropy-alloy design concept, the potential of $Al_{0.5}CoCrCuFeNi$ alloy can be explored further with suitable composition modification. In consideration of the strong bonding between vanadium and many metal elements, vanadium addition to the $Al_{0.5}CoCrCuFeNi$ alloy was investigated in the current study to improve its mechanical performance. The results show that vanadium can promote the alloy's performance, revealing a high potential for the application to the tool alloy industry.

## II. EXPERIMENTAL DETAILS

The $Al_{0.5}CoCrCuFeNiV_x$ high-entropy alloys with different vanadium contents ($x = 0$ to 2.0 in the ratio of alloying element moles) were prepared in this study by the arc melting and casting method. The method followed the same procedure as described in Reference 7. The alloy specimens were polished and etched with *aqua regia* for observation under an optical microscope and scanning electron microscope (SEM; JEOL* JSM-5410). The chemical

MIN-RUI CHEN, Postgraduate Student, SU-JIEN LIN, Professor, JIEN-WEI YEH, Professor, and MING-HAO CHUANG, Ph.D. Student, are with the Department of Materials Science and Engineering, National Tsing Hua University, Hsinchu 300, R.O.C. Taiwan. Contact e-mail: jwyeh@mx.nthu.edu.tw SWE-KAI CHEN, Professor, is with the Materials Science Center, National Tsing Hua University, Hsinchu 300, R.O.C. Taiwan. YUAN-SHENG HUANG, Professor, is with the Department of Mechanical and Electronic Engineering, Shaoguan University, Shaoguan City, Guangdong 512005, P.R. China.

Manuscript submitted April 2, 2005.

*JEOL is a trademark of Japan Electron Optics Ltd., Tokyo.

compositions of different phases were analyzed by SEM energy dispersive spectrometry (EDS). An X-ray diffractometer (XRD; Rigaku ME510-FM2, Tokyo, Japan) was used to identify the crystalline structure, with the $2\theta$ scan ranging from 20 to 100 deg at a speed of 1 deg/min. The typical radiation condition was 30 kV and 20 mA with a copper target. Hardness measurements were conducted using a Vickers hardness tester (Matsuzawa Seiki MV-1) under a load of 49 N and at a loading speed of 70 $\mu$m/sec for 20 seconds. Every specimen was measured five times. Scattering errors were within 3 pct. Wear resistance was measured with a modified pin-on-disk dry wear tester under the load of 29.4 N without any lubrication. The modified pin-on-disk dry wear tester was described in Reference 8. The sliding velocity of wear-test sand belts attached with 149-$\mu$m alumina ($Al_2O_3$) particles was controlled at 0.5 m/sec for a sliding distance of 20 m. Test pins of the alloys with a diameter of 8 mm were controlled to move perpendicular to the sand-belt motion to avoid repeating wear tracks and to obtain highly reproducible data. The weight loss of the pins after wear tests was measured, divided by the alloy density and the sliding distance, and inversed to obtain the wear resistance.

## III. RESULTS AND DISCUSSION

### A. *Effect of Vanadium Addition on Microstructure*

Figure 1 shows the XRD patterns of $Al_{0.5}CoCrCuFeNiV_x$ as-cast alloys. The crystal structures of $Al_{0.5}CoCrCuFeNiV_x$ alloy system are characterized, and only simple solid-solution structures, essentially fcc, bcc, and $\sigma$ phase, are identified, in which $\sigma$ phase forms from $x = 0.6$ to 1.0. $Al_{0.5}CoCrCuFeNiV_{0.2}$, similar to $Al_{0.5}CoCrCuFeNi$, is of fcc structure. The bcc phase begins to appear at $x = 0.4$, and its amount increases with vanadium content increase up to $x = 2.0$. It is obvious that $Al_{0.5}CoCrCuFeNiV_x$ alloy is composed of fcc phase and bcc phase when the vanadium content is $x = 0.4$, composed of fcc phase, bcc phase, and $\sigma$ phase when the vanadium content is between $x = 0.6$ and 1.0, and composed of fcc phase and bcc phase when the vanadium content exceeds 1.0. $\sigma$ phase is a multielement solid-solution phase having the same structure as equal-mole NiCoCr phase in accordance with the Powder Diffraction File edited by International Center for Diffraction Data. EDS analysis shows that $\sigma$ phase also contains a higher amount of vanadium than other phases in matrix. Moreover, the amount of $\sigma$ phase increases with increasing vanadium content from 0.6 to 1.0.

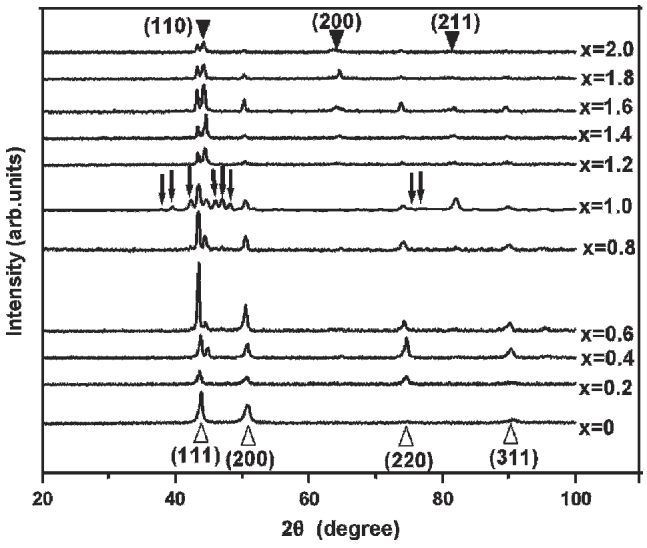


Fig. 1—XRD analyses of $Al_{0.5}CoCrCuFeNiV_x$ alloys with different vanadium contents ($x$ value in molar ratio). Δ, fcc phase; ▼, bcc phase; ↓, $\sigma$ phase.

Figures 2, 3, and 4 show the SEM microstructures of as-cast $Al_{0.5}CoCrCuFeNiV_x$ alloys with different vanadium contents. Typical cast dendrite and interdendrite structures (DR and ID in the figures, respectively) are observed in these alloys. It is obvious that the effect of vanadium on the alloy structure is little at the vanadium content of 0.2. Both the dendrites and interdendrites still belong to fcc phases with the same lattice constants (Figures 2(a) and (b)), for the XRD pattern of $Al_{0.5}CoCrCuFeNiV_{0.2}$ shows only one fcc structure (Figure 1). When the vanadium content is between 0.4 and 0.8, the dendrites are divided into two zones (A and B), as shown in Figures 2(c) to (f) and Figures 3(a) and (b). Zone A, similar to the dendrite of $Al_{0.5}CoCrCuFeNiV_{0.2}$, is of fcc structure, whereas zone B is of bcc structure, as verified by X-ray analysis and EDS analysis. Zone B further reveals spinodal decomposition (indicated by SD) structure, which shows different morphologies at different vanadium contents. Similar spinodal decomposition with different morphologies for bcc phase has been reported and discussed with SEM and transmission electron microscopy (TEM) investigation for $Al_yCoCrCuFeNi$ alloys ($y = 0$ to 3.0) in previous work.[9] The precipitates in zone B are spherical at $x = 0.4$, both spherical and plate-like at $x = 0.6$, and mostly plate-like at $x = 0.8$—*i.e.*, the precipitates gradually change morphology from spherical to plate-like. Needle-like widmanstätten structure (Figures 3(b) and (d)) coexists with spinodal structure. This needle-like phase is believed to be $\sigma$ phase because its formation and amount coincide with the appearance of $\sigma$ phase in X-ray patterns. To verify the composition of the needle-like phase, EDS line scanning was used; the results show that it is rich in vanadium compared to the other matrix phases. It is clear that the volume fraction of zone B increases as vanadium content increases from 0.4 to 0.8. As the vanadium content reaches 1.0, zone A disappears in the dendrite region—*i.e.*, the dendrite is composed only of bcc phase and the Cu-rich interdendrite is of fcc phase, in accordance with X-ray analysis. This trend toward the formation of bcc phase is very reasonable since vanadium is a well-known bcc former or stabilizer.

The alloys were also analyzed with TEM. The results of a typical alloy, $Al_{0.5}CoCrCuFeNi$, are shown in detail. As confirmed by TEM bright-field image and corresponding SAD pattern shown in Figure 5(a), the dendrite of cast $Al_{0.5}CoCrCuFeNi$ alloy, presented in Figure 2(a), is composed of fcc structure. No special feature except a strain-field–induced modulated structure formed during TEM sample preparation is observed. Moreover, an ordered fcc phase with some degree of ordering was revealed by the SAD pattern precipitates at the sizes of 5 to 10 nm (bright spots) within the disordered matrix during solidification, as

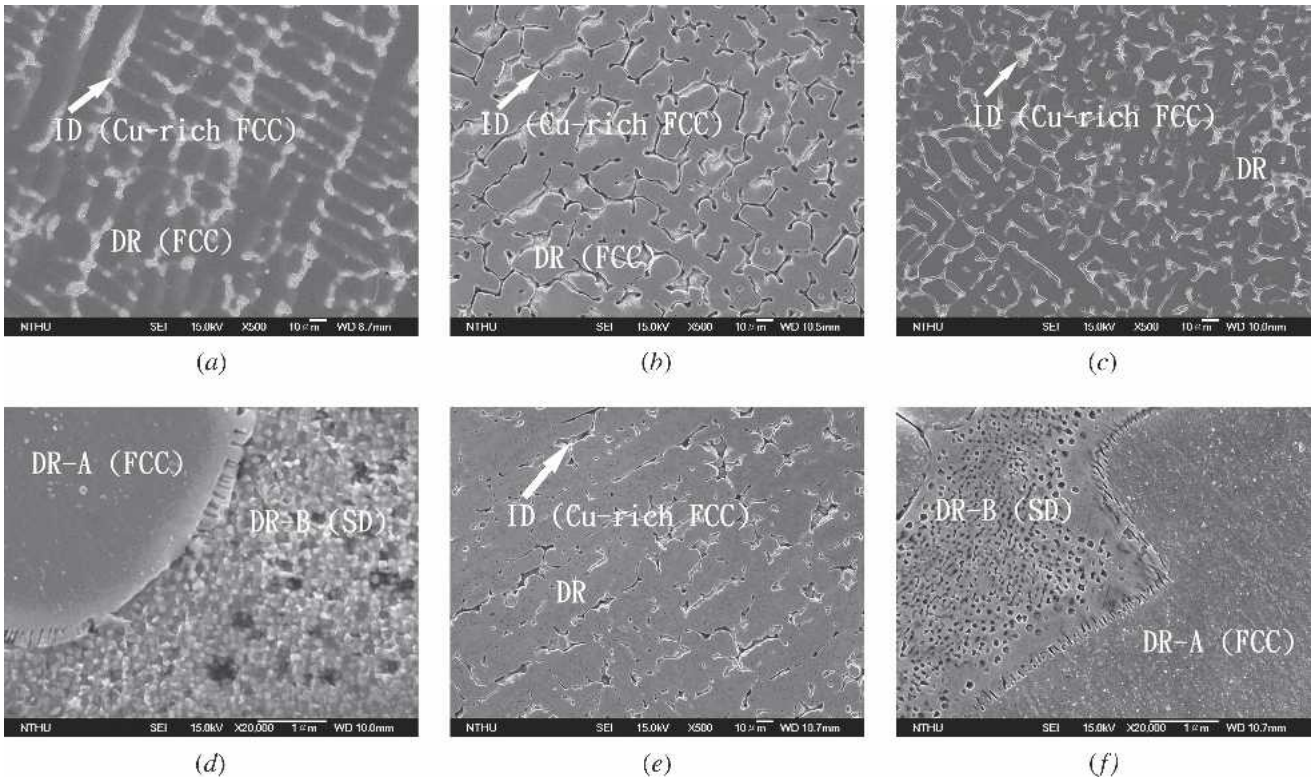


Fig. 2—SEM microstructures of as-cast $Al_{0.5}CoCrCuFeNiV_x$ alloys with different vanadium contents ($x$ value): (*a*) 0, (*b*) 0.2, (*c*) 0.4, (*d*) 0.4 (dendrite region), (*e*) 0.6, and (*f*) 0.6 (dendrite region). DR, dendrite; ID, interdendrite; SD, spinodal decomposition.

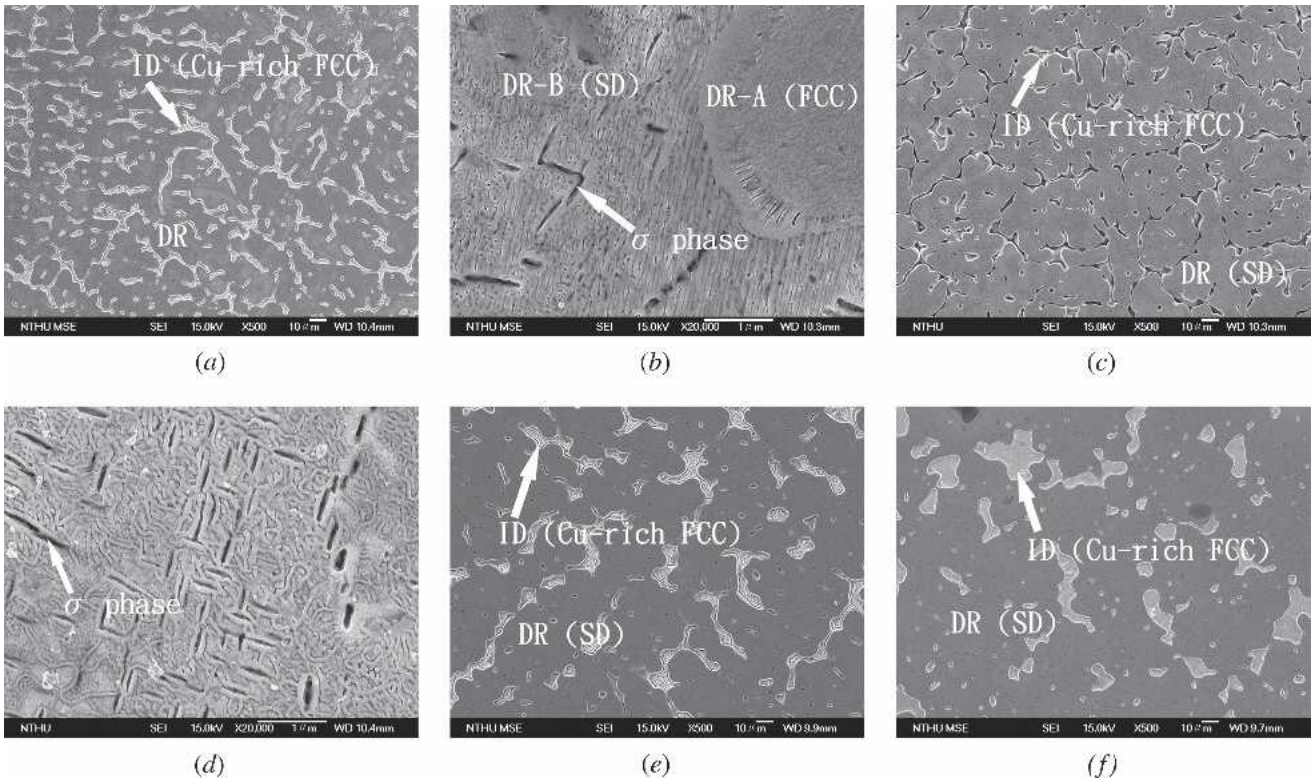


Fig. 3—SEM microstructures of as-cast $Al_{0.5}CoCrCuFeNiV_x$ alloys with different vanadium contents ($x$ value): (*a*) 0.8, (*b*) 0.8 (dendrite region), (*c*) 1.0, (*d*) 1.0 (dendrite region), (*e*) 1.2, and (*f*) 1.4.

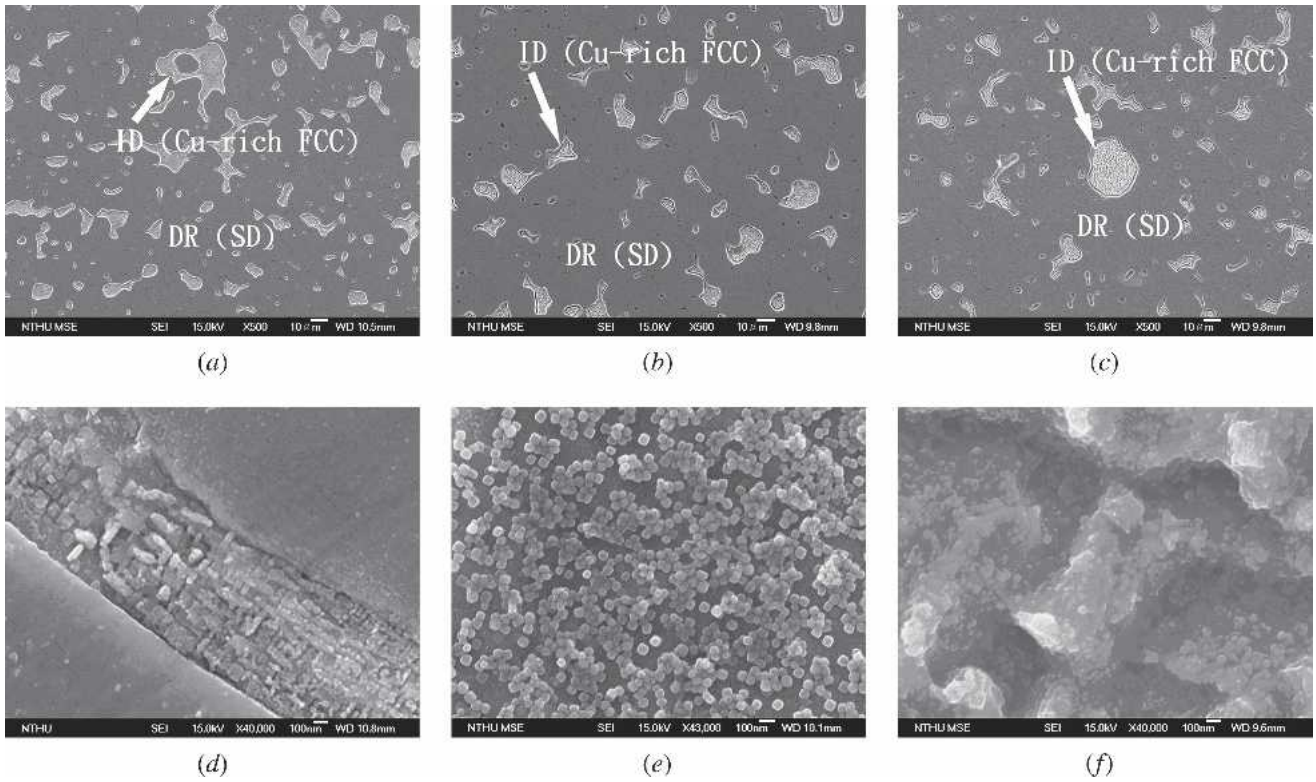


Fig. 4—SEM microstructures of as-cast $Al_{0.5}CoCrCuFeNiV_x$ alloys with different vanadium contents ($x$ value): (*a*) 1.6, (*b*) 1.8, (*c*) 2.0, (*d*) 0.2 (interdendrite region), (*e*) 1.0 (interdendrite region), and (*f*) 2.0 (interdendrite region).

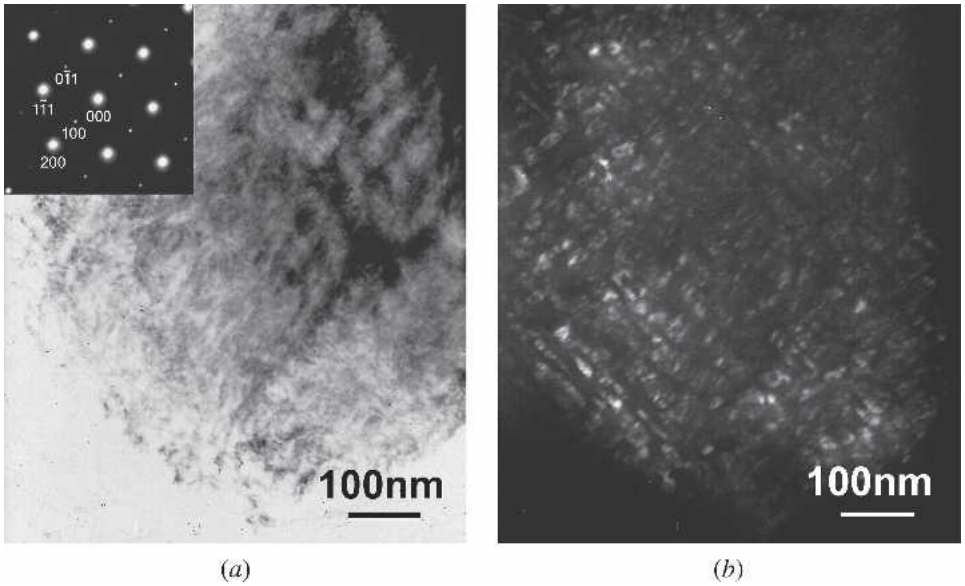


Fig. 5—TEM microstructures of the dendrite of as-cast $Al_{0.5}CoCrCuFeNi$ alloy. (*a*) Bright-field image with SAD pattern of fcc [011] zone axis. (*b*) Dark-field image corresponding to the (100) superlattice spot of the SAD pattern shown in (*a*).

seen in Figure 5(b), a TEM dark-field image. As for the bcc phase and its spinodal structure of the alloys with vanadium content above $x = 0.4$, the TEM microstructure is similar to that observed in alloys with aluminum content above $x = 1.0$ in the previous work.[9]

The chemical compositions of the cast alloys were analyzed by EDS, and the results are summarized in Table I. Although copper segregation at the interdendrite regions is observed, the dendrites of large volume fractions are basically composed of multiprincipal elements and thus have similar concentration to the total concentration, except copper. With the increase of the content of vanadium, more and more copper segregates to the interdendrite region. This is because the mixing enthalpy for a mixture of copper

**Table I. Chemical Compositions of Cast $Al_{0.5}CoCrCuFeNiV_x$ Alloys**

| Alloy | Element (At. Pct) | | | | | | |
|---|---|---|---|---|---|---|---|
| | Al | Cr | Cu | Fe | Co | Ni | V |
| $Al_{0.5}CoCrCuFeNi$ | | | | | | | |
| Total | 9.09 | 18.18 | 18.18 | 18.18 | 18.18 | 18.18 | |
| Dendrite | 9.4 | 19.5 | 12.6 | 19.4 | 18.7 | 20.4 | |
| Interdendrite | 12.5 | 4.1 | 61.3 | 4.7 | 5.2 | 12.2 | |
| $Al_{0.5}CoCrCuFeNiV_{0.2}$ | | | | | | | |
| Total | 8.7 | 17.5 | 17.5 | 17.5 | 17.5 | 17.5 | 3.5 |
| Dendrite | 7.4 | 21.1 | 9.4 | 19.3 | 20.2 | 18.4 | 4.2 |
| Interdendrite | 13.6 | 3.2 | 62.8 | 3.8 | 4.2 | 12.0 | 0.4 |
| $Al_{0.5}CoCrCuFeNiV_{0.4}$ | | | | | | | |
| Total | 8.4 | 16.9 | 16.9 | 16.9 | 16.9 | 16.9 | 6.7 |
| Dendrite (A) | 7.3 | 19.1 | 8.9 | 19.4 | 19.7 | 17.9 | 7.7 |
| Dendrite (B) | 8.9 | 26.2 | 6.7 | 18.2 | 17.3 | 13.3 | 9.4 |
| Interdendrite | 12.7 | 3.4 | 60.3 | 4.2 | 4.6 | 13.8 | 1.0 |
| $Al_{0.5}CoCrCuFeNiV_{0.6}$ | | | | | | | |
| Total | 8.1 | 16.3 | 16.3 | 16.3 | 16.3 | 16.3 | 9.8 |
| Dendrite (A) | 7.1 | 17.3 | 9.4 | 17.8 | 18.6 | 19.5 | 10.3 |
| Dendrite (B) | 7.8 | 22.8 | 5.9 | 18.2 | 17.9 | 14.3 | 13.1 |
| Interdendrite | 11.8 | 2.6 | 68.1 | 2.9 | 2.8 | 11.3 | 0.5 |
| $Al_{0.5}CoCrCuFeNiV_{0.8}$ | | | | | | | |
| Total | 7.9 | 15.8 | 15.8 | 15.8 | 15.8 | 15.8 | 12.6 |
| Dendrite (A) | 7.1 | 14.6 | 11.5 | 16.1 | 17.9 | 20.6 | 12.2 |
| Dendrite (B) | 7.3 | 19.7 | 7.5 | 16.6 | 18.3 | 15.4 | 15.2 |
| Interdendrite | 11.6 | 2.6 | 63.7 | 3.2 | 4.4 | 12.9 | 1.6 |
| $Al_{0.5}CoCrCuFeNiV_{1.0}$ | | | | | | | |
| Total | 7.6 | 15.3 | 15.3 | 15.3 | 15.3 | 15.3 | 15.3 |
| Dendrite | 7.2 | 17.6 | 9.5 | 15.3 | 16.8 | 17.2 | 16.4 |
| Interdendrite | 11.8 | 2.8 | 61.2 | 3.4 | 4.0 | 14.3 | 2.5 |
| $Al_{0.5}CoCrCuFeNiV_{1.2}$ | | | | | | | |
| Total | 7.4 | 14.9 | 14.9 | 14.9 | 14.9 | 14.9 | 17.9 |
| Dendrite | 6.4 | 18.1 | 5.9 | 16.0 | 17.1 | 15.0 | 21.5 |
| Interdendrite | 10.7 | 2.4 | 66.4 | 2.9 | 3.1 | 12.2 | 2.3 |
| $Al_{0.5}CoCrCuFeNiV_{1.4}$ | | | | | | | |
| Total | 7.2 | 14.4 | 14.4 | 14.4 | 14.4 | 14.4 | 20.2 |
| Dendrite | 5.2 | 18.3 | 5.8 | 15.3 | 17.0 | 14.0 | 24.4 |
| Interdendrite | 11.7 | 1.6 | 68.9 | 1.9 | 2.2 | 12.5 | 1.2 |
| $Al_{0.5}CoCrCuFeNiV_{1.6}$ | | | | | | | |
| Total | 7.0 | 14.1 | 14.1 | 14.1 | 14.1 | 14.1 | 22.5 |
| Dendrite | 6.1 | 16.6 | 6.4 | 14.3 | 15.8 | 15.1 | 25.7 |
| Interdendrite | 11.7 | 1.1 | 74.0 | 1.5 | 1.9 | 8.6 | 1.2 |
| $Al_{0.5}CoCrCuFeNiV_{1.8}$ | | | | | | | |
| Total | 6.8 | 13.7 | 13.7 | 13.7 | 13.7 | 13.7 | 24.6 |
| Dendrite | 5.9 | 16.5 | 5.5 | 13.4 | 15.8 | 14.6 | 28.3 |
| Interdendrite | 10.8 | 1.2 | 73.5 | 1.5 | 1.7 | 9.8 | 1.5 |
| $Al_{0.5}CoCrCuFeNiV_{2.0}$ | | | | | | | |
| Total | 6.6 | 13.3 | 13.3 | 13.3 | 13.3 | 13.3 | 26.6 |
| Dendrite | 5.7 | 16.7 | 5.1 | 13.2 | 15.0 | 13.8 | 30.5 |
| Interdendrite | 12.5 | 1.1 | 74.9 | 0.9 | 1.4 | 8.2 | 1.0 |

and vanadium is 5 kJ/mole, whereas those for a mixture of vanadium and (separately) aluminum, cobalt, chromium, iron, and nickel are −16, −14, −2, −7, and −18 kJ/mole, respectively.[11] That means that copper dislikes living in dendrite with a higher vanadium concentration. Copper concentrations in all interdendrite regions are more than 60 at. pct, and the concentrations of Al and Ni are next, each around 15 at. pct. This is reasonable, since Al and Ni have greater chemical affinity with Cu than Co, Cr, Fe, and V. The chemical analysis of zone A and zone B coexisting when the vanadium content is between 0.4 and 0.8 may be used to identify their individual crystal structure. Since the concentrations of bcc formers Al, Cr, Fe, and V in zone B are more than that in zone A, while the concentrations of fcc former Cu and Ni in zone A are more than that in zone B, it follows that zone A is of fcc phase while zone B is of bcc phase.

The interdendrite region mainly consists of fcc phase, since EDS analysis shows that it contains more than 60 pct copper. This is similar to that reported in Cu-bearing high-entropy alloys.[9] It is obvious that numerous nanoparticles having a size of 50 nm can be seen in the interdendrite. Figures 4(d) to (f) show the typical nanoparticle morphologies. A high concentration of other elements in these

Cu-rich regions may account for the nanoprecipitation due to their sluggish cooperative diffusion.[7,9] The net-like morphology of the interdendrite region drastically changes into an island-like structure (Figures 3(e) and (f) and Figures 4(a) to (c)) when the vanadium content increases from 1.2 to 2.0. Within this range of vanadium content, the microstructures show little difference.

### B. *Effect of Vanadium Addition on Hardness*

Figure 6 shows the Vickers hardness of the $Al_{0.5}CoCrCuFeNiV_x$ alloy system as a function of vanadium content. When the vanadium content is less than 0.4, the effect of vanadium on the hardness of the alloys is small. With more vanadium addition, the hardness value rapidly increases and peaks (640 HV) at $x = 1.0$. When the vanadium content increases from 1.0 to 1.2, the hardness value is reduced to 576 HV; moreover, the hardness is almost unchanged when the vanadium content is increased further. The Vickers microhardness tester was used to measure the hardness of the dendrite and interdendrite regions of the alloys. The results show that the hardness of dendrite is beween 295 and 998 HV, depending on the phase structure. When $x = 0.2$, the hardness of dendrite, which is of fcc phase, is 295 HV. When $x = 1.0$, the hardness of dendrite, which consists of bcc and $\sigma$ phases, peaks at 998 HV. When $x = 2.0$, the hardness of dendrite, which is of bcc phase, is 749 HV. That of Cu-rich FCC interdendrite is around 150 HV. Therefore, in comparison with the microstructural evolution shown in Figure 6, the increased volume fraction of bcc phase relative to that of bcc phase is the most important factor of strengthening, and the increased $\sigma$ phase precipitation between $x = 0.6$ and 1.0 is the next.

In the ranges of $x \leq 0.4$ and $x \geq 1.2$, solution hardening in fcc and bcc phases seems small with the addition of more vanadium. This is reasonable, since in these solution phases there is no matrix element and all atoms may be regarded as solute atoms, and as a result they are of highly concentrated solid solution and show little sensitivity to the incorporation of other atoms with similar bonding strength.[4] The phenomenon that the bcc phase is stronger than fcc phase was also reported in the previous work on the $Al_yCoCrCuFeNi$ alloys ($y = 0$ to 3.0).[4,10] It can be explained based on three viewpoints. The first is the fact that slip along the closest packing planes {110} in bcc structure is more difficult than that along those {111} in bcc structure, because {110} planes are less dense and more irregular than {111} planes in the atomic scale and possess a smaller interplanar spacing and higher lattice friction gliding. The second is due to the incorporation of more atoms in bcc phase with a stronger binding element like Al and high-melting-point elements like Cr, V to increase the slip resistance. The third is the spinodal decomposition of BCC phase by which a nano-spaced spinodal structure (Figures 2(d) and (f) and Figure 3(b)) may also provide a nanocomposite strengthening effect.[4,9] Apart from the contribution of bcc phase formation, the enhanced hardness increase in the range of $x = 0.6$ to 1.0 is relevant to $\sigma$ phase formation. With the vanadium content increase from 0.6 to 1.0, the amount of $\sigma$ phase increases and causes the hardness value to rise sharply and peak at $x = 1.0$. Then the hardness value decreases at the vanadium content of 1.2, where $\sigma$ phase disappears. This phenomenon reflects that $\sigma$ phase, being an intermetallic compound, has a higher hardness than bcc phase. Therefore, we can conclude that $\sigma$ phase also provides an effective precipitation hardening.

### C. *Effect of Vanadium Addition on Wear Resistance*

The effect of vanadium addition on the wear resistance of $Al_{0.5}CoCrCuFeNi$ alloys is shown in Figure 6. When the content of vanadium is less than 0.6, the wear resistance of the $Al_{0.5}CoCrCuFeNiV_x$ alloys is much the same as that of $Al_{0.5}CoCrCuFeNi$. However, the wear resistance is significantly enhanced when the vanadium content increases by around 20 pct, from 0.6 to 1.2. After the vanadium content exceeds 1.2, the wear resistance has almost no increase, similar to that of $Al_{0.5}CoCrCuFeNiV_{1.2}$ alloy. Thus, the optimal vanadium addition for tool applications is between $x = 1.0$ and 1.2. Figure 7 shows the correlation between wear resistance and hardness. From the wear resistance analysis as shown in Figures 6 and 7, we find that the wear resistance of $Al_{0.5}CoCrCuFeNiV_x$ alloys is seemingly

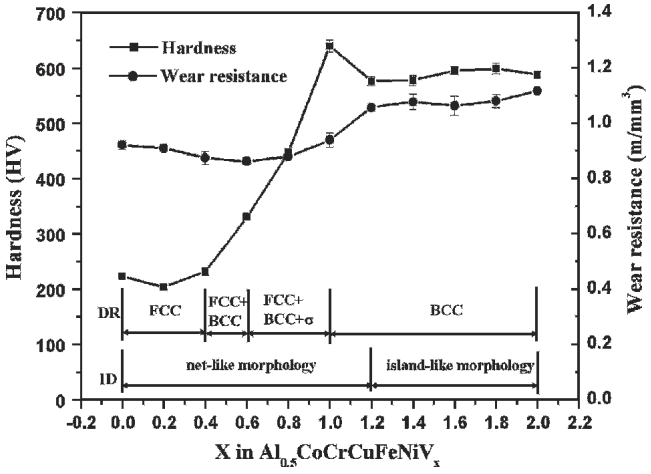


Fig. 6—Vickers hardness and wear resistance of $Al_{0.5}CoCrCuFeNiV_x$ alloys with different vanadium contents.

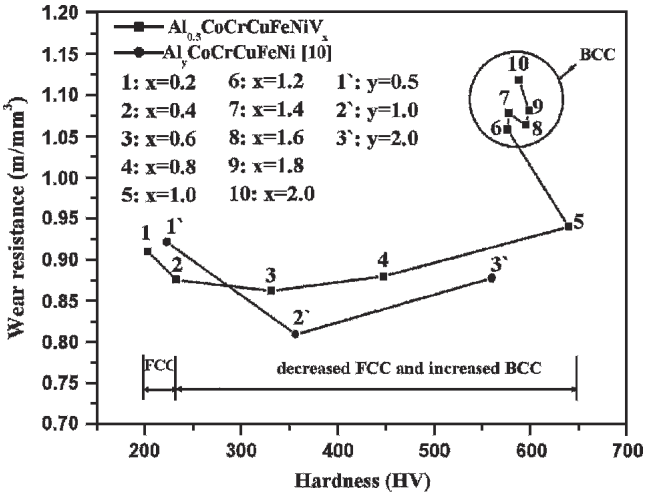


Fig. 7—Wear resistance *vs* hardness of $Al_{0.5}CoCrCuFeNiV_x$ and $Al_yCoCrCuFeNi$ alloys.

insensitive to their hardness in the transition from fcc phase to bcc phase. In general, the wear resistance of materials is proportional to their Vickers hardness.[12] However, the wear resistance of $Al_{0.5}CoCrCuFeNiV_x$ alloys does not follow linearly the hardness, as seen in Figure 7.

Our previous investigations[8,10] have shown that the fcc structure of high-entropy alloys $Al_{0.5}CoCrCuFeNi$ exhibit excellent work-hardening capability, which raises the as-cast hardness around 200 HV to the as-rolled one around 400 HV and thus results in a good wear resistance. Reference 10 also reported that an increased amount of stronger bcc phase due to more Al addition does not significantly increase the wear resistance, as shown in Figure 7. The current study found similar phenomenon from the vanadium content $x = 0$ to 0.6—*i.e.*, although the volume fraction of stronger bcc phase increases, its benefit in wear resistance is not seen. Both observations reflect the fact that the bcc phases substituting the fcc phase with large work-hardening capacity will not have an even higher hardness than the full-hard state of fcc phase. In contrast, for the enhanced wear resistance that occurs when the vanadium content exceeds 0.6, the phases substituting the FCC phase would have higher hardness than that of full-hard fcc phase. This has been verified by the microhardness measurement as mentioned in Section III–B, in which bcc phase at $x = 2.0$ could have a hardness of 749 HV, and bcc phase plus $\sigma$ phase at $x = 1.0$ could have an even higher hardness of 998 HV.

The wear resistances of $Al_yCoCrCuFeNi$ alloys with different aluminum content ($y$ value in molar ratio) and those of $Al_{0.5}CoCrCuFeNiV_x$ alloys, as shown in Figure 7, were also compared for the effect of aluminum and vanadium additions. As the content of the added elements exceeds 0.5, the contribution of increasing vanadium content to wear resistance is better than that of increasing aluminum content. This is attributable to the different ordering tendency exerted by aluminum and vanadium. Aluminum tends to render bcc phase more highly ordered, as revealed by the ordered bcc peak at 31 deg in their X-ray patterns, and thus more brittle. Therefore, compared with $Al_yCoCrCuFeNi$, the vanadium addition to the $Al_{0.5}CoCrCuFeNi$ alloys obviously promotes the alloy properties further.

## IV. CONCLUSIONS

With little vanadium addition, the $Al_{0.5}CoCrCuFeNiV_x$ alloys were composed of a simple fcc solid-solution structure. As the vanadium content reaches 0.4, a bcc structure appears with spinodal decomposition and envelops the fcc dendrites. From $x = 0.4$ to 1.0, the volume fraction of bcc structure phase increases with the vanadium content increase. When $x = 1.0$, fcc dendrites become completely replaced by bcc dendrites. Needle-like $\sigma$ phase forms in the bcc spinodal structure and increases from $x = 0.6$ to 1.0 but disappears from $x = 1.2$ to 2.0. The hardness and wear resistance of the alloys were tested, and changes were found with the evolution of the microstructure. The hardness values of the alloys increase when the vanadium content is increased from 0.4 to 1.0 and peak (640 HV) at a vanadium content of 1.0. The wear resistance increases by around 20 pct as the vanadium content increases from $x = 0.6$ to 1.2 and levels off beyond $x = 1.2$. The optimal vanadium addition is between $x = 1.0$ and 1.2. Compared with the previous investigation of $Al_{0.5}CoCrCuFeNi$ alloy, adding vanadium to the alloy promotes the alloy properties.

## ACKNOWLEDGMENTS

The authors gratefully acknowledge the financial support for this research by the National Science Council of Taiwan under grant no. NSC-91-2120-E-007-007 and the Ministry of Economic Affairs of Taiwan under grant no. 92-CE-17-A-08-S1-0003.

## REFERENCES

1. Handbook Committee: *Metals Handbook*, 10th ed., vol. 1, ASM International, Metals Park, OH, 1990.
2. Handbook Committee: *Metals Handbook*, 10th ed., vol. 2, ASM International, Metals Park, OH, 1990.
3. A.L. Greer: *Nature*, 1993, vol. 366, pp. 303-04.
4. J.W. Yeh, S.K. Chen, S.J. Lin, J.Y. Gan, T.S. Chin, T.T. Shun, C.H. Tsau, and S.Y. Chang: *Adv. Eng. Mater.*, 2004, vol. 6, pp. 299-303.
5. S. Ranganathan: *Curr. Sci.*, 2003, vol. 85, pp. 1404-06.
6. R.A. Swalin: *Thermodynamics of Solids*, 2nd ed., E. Burke, B. Chalmers, J.A. Krumhansl, eds., John Wiley & Sons, New York, NY, 1991, pp. 21-87.
7. P.K. Huang, J.W. Yeh, T.T. Shun, and S.K. Chen: *Adv. Eng. Mater.*, 2004, vol. 6, pp. 74-78.
8. C.Y. Hsu, J.W. Yeh, S.K. Chen, and T.T. Shun: *Metall. Mater. Trans. A*, 2004, vol. 35A, pp. 1465-69.
9. C.J. Tong, Y.L. Chen, S.K. Chen, J.W. Yeh, T.T. Shun, C.H. Tsau, S.J. Lin, and S.Y. Chang: *Metall. Mater. Trans. A*, 2005, vol. 36A, pp. 881-93.
10. C.J. Tong, M.R. Chen, S.K. Chen, J.W. Yeh, T.T. Shun, S.J. Lin, and S.Y. Chang: *Metall. Mater. Trans. A*, 2005, vol. 36A, pp. 1263-71.
11. F.R. de Boer, R. Boom, W.C.M. Mattens, A.R. Miedema, and A.K. Nissen: *Cohesion in Metals*, Elsevier Science Publishing Company, 1989.
12. M.M. Khruschov: *Wear*, 1974, vol. 28, pp. 69-88.